ELSEVIER

Polymer 43 (2002) 1357–1364

polymer

www.elsevier.com/locate/polymer

Miscibility and morphology in crystalline/amorphous blends of poly(caprolactone)/poly(4-vinylphenol) as studied by DSC, FTIR, and ^{13}C solid state NMR

Jian Wang[a], Man Ken Cheung[b], Yongli Mi[a,*]

[a]*Department of Chemical Engineering, The Hong Kong University of Science and Technology, Clear Water Bay, Kowloon, Hong Kong*
[b]*Department of Applied Biology & Chemical Technology, The Hong Kong Polytechnic University, Hung Hom, Kowloon, Hong Kong*

Received 4 May 2001; received in revised form 27 September 2001; accepted 28 September 2001

Abstract

The miscibility and morphology of poly(caprolactone) (PCL) and poly (4-vinylphenol) (PVPh) blends were investigated by using differential scanning calorimetry (DSC), Fourier transform infrared (FTIR) spectroscopy and ^{13}C solid state nuclear magnetic resonance (NMR) spectroscopy. The DSC results indicate that PCL is miscible with PVPh. FTIR studies reveal that hydrogen bonding exists between the hydroxyl groups of PVPh and the carbonyl groups of PCL. ^{13}C cross polarization (CP)/magic angle spinning (MAS)/dipolar decoupling (DD) spectra of the blends show a 1 ppm downfield shifting of ^{13}C resonance of PVPh hydroxyl-substituted carbons and PCL carbonyl carbons with increasing PCL content. Both FTIR and NMR give evidence of inter-molecular hydrogen bonding within the blends. The proton spin–lattice relaxation in the laboratory frame, $T_1(H)$, and in the rotating frame, $T_{1\rho}(H)$, were studied as a function of the blend composition. The $T_1(H)$ results are in good agreement with thermal analysis; i.e. the blends are completely homogeneous on the scale of 50–80 nm. The $T_{1\rho}(H)$ results indicate that PCL in the blends has both crystalline and amorphous phases. The amorphous PCL phase is miscible with PVPh, but the PCL crystal domain size is probably larger than the spin–diffusion path length within the $T_{1\rho}(H)$ time-frame, i.e. larger than 2–4 nm. The mobility differences between the crystalline and amorphous phases of PCL are clearly visible from the $T_{1\rho}(H)$ data.

Keywords: Poly(caprolactone), PCL; Poly(4-vinylphenol), PVPh; Polymer blends

1. Introduction

Binary polymer blends can be categorized into amorphous/amorphous, crystalline/amorphous, and crystalline/crystalline systems. Among these systems, blending an amorphous polymer with a crystalline polymer is a convenient way of improving the impact strength, toughness, ductility and other physical properties since the occurrence of liquid–solid interface can offer an effective route to produce a wide variety of morphological patterns. Although the miscibility and morphological structures of crystalline/amorphous polymer blends have been widely investigated [1–10], some basic principles are still not well understood, like the segregation between the crystalline/amorphous interface, the relationship of the specific inter-molecular interactions and the domain size of the separated phases.

High-resolution solid state nuclear magnetic resonance (NMR) spectroscopy of polymer blends can reveal detailed information about the miscibility, inter-molecular interaction, and domain size by examining NMR parameters such as chemical shift, line width, and relaxation parameters. High-resolution spectra, obtained by the combination of cross polarization (CP) with magic angle sample spinning (MAS) and proton decoupling (DD), reveal not only the primary repeating unit structure but also the different conformations [11–15]. Spin–lattice relaxation times in the laboratory frame, $T_1(H)$, and in the rotating frame, $T_{1\rho}(H)$, are sensitive to the mobility of polymer chains. Domain size is commonly estimated via the spin diffusion process.

In this study, polymer blends of semi-crystalline poly(caprolactone) (PCL) and amorphous poly(4-vinylphenol) (PVPh) were investigated. Poly(caprolactone) has been known to be miscible with polymers, like poly(vinyl chloride) (PVC) [4], copolymer of styrene and acrylonitrile (SAN) [10], poly(benzyl methacrylate) (PBMA) [9], and poly(vinyl alcohol) (PVA) [5], because the carbonyl group

* Corresponding author. Fax: +852-358-0054.
E-mail address: keymix@usthk.ust.hk (Y. Mi).

0032-3861/02/$ - see front matter
PII: S0032-3861(01)00673-5

of PCL can form inter-molecular interaction with other polar functional groups. Poly(4-vinylphenol) is similar to polystyrene, but possesses a hydroxyl group attached to the aromatic ring. PVPh can act as a proton donor that forms hydrogen bonds with proton acceptor polymers [16–21]. In this study, the miscibility and morphology of PCL/PVPh blends were investigated by several techniques. Differential scanning calorimetry (DSC) was applied to study the glass and melting behaviours, Fourier transform infrared (FTIR) spectroscopy was used to analyse the specific interactions between the components, and ^{13}C solid state NMR techniques was employed to study the morphology and domain size of PCL/PVPh blends.

2. Experimental

2.1. Materials and preparation of samples

Poly(caprolactone) (PCL) was purchased from Aldrich Chemical Company, Inc. (Milwaukee, WI, USA), with $M_n = 80,000\ g\ mol^{-1}$. Poly (4-vinylphenol) (PVPh), with an approximate $M_w = 22,000\ g\ mol^{-1}$, was purchased from Polysciences, Inc. (Warrington, PA, USA). The as-received materials were free of additives and were used without further purification.

The blends were prepared by casting 2.5% (w/v) THF solution. The solvent evaporated slowly at room temperature for one week, followed by removal of residual solvent in a vacuum oven for one more week at 50°C.

2.2. Differential scanning calorimetry

The calorimetric measurements were carried out by a Perkin–Elmer Pyris 1 differential scanning calorimeter. Sub-ambient temperatures were reached by using a mechanical intra-cooler. The instrument was calibrated with indium and zinc standards for low and high temperature regions, respectively. The midpoint of the slope change of the heat capacity was taken as glass transition temperature (T_g). The melting point of each endotherm was located in the maximum of their respective peaks.

All blend samples were heated from −65 to 180°C for the first scan, and were maintained at 180°C for two minutes to ensure complete melting of PCL crystals. After that, the samples were quenched to −65°C at the rate of 100°C min^{-1}, and were heated again from −65 to 180°C. A heating rate of 20°C min^{-1} was used.

2.3. Fourier-transform infra-red spectroscopy

FTIR spectra were obtained using a Bio-rad FTS6000 spectrometer. Thin films of the blends were cast onto NaCl windows from 0.5% (w/v) THF solutions. After evaporating most of the solvent at room temperature, they were transferred to a vacuum oven and kept at 50°C for 1 week to remove the residual solvent and then stored in a desiccator to avoid moisture adsorption. All spectra were recorded at room temperature. A minimum of 128 scans at a resolution of $2\ cm^{-1}$ was signal averaged. The films used in this study were sufficiently thin to obey the Beer–Lambert law.

2.4. Solid state NMR

High-resolution solid state NMR experiments were carried out at ambient temperature (27°C) on a JEOL JNM-EX400 FT NMR spectrometer at the resonance frequencies of 399.65 MHz for ^1H and 100.40 MHz for ^{13}C. The high-resolution ^{13}C solid state NMR spectra were obtained using the technique of CP with MAS and high-power dipolar decoupling (DD). The ^1H 90° pulse width was 5.5 μs. The CP Hartmann–Hahn contact time was set at 1.0 ms for all experiments since the experiments demonstrated that the contact time is suitable for the detection of CP/MAS/DD spectra for both the pure components and the blends. The sample-spinning rate was 5.0–5.4 kHz for all NMR measurements. ^{13}C total sideband suppression (TOSS) spectra were obtained using a scheme that is depicted in Fig. 1(a). The ^{13}C chemical shift scale was set with a solid external reference standard, adamantane (ADM), which has two resonant peaks at 29.5 and 38.6 ppm, relative to tetramethylsilane (TMS).

The proton spin–lattice relaxation time in the laboratory frame, $T_1(H)$, was measured by monitoring the protonated carbon resonance intensities at different delay τ in a ^1H π–τ–$\pi/2$ inversion–recovery scheme before CP to ^{13}C (Fig. 1(b)). The proton spin–lattice relaxation time in the rotating frame, $T_{1\rho}(H)$, was measured by monitoring the protonated carbon signal intensities at different ^1H spin-lock durations prior to CP (Fig. 1(c)).

3. Results and discussion

3.1. Differential scanning calorimetry (DSC)

The DSC thermograms (the second heating scan) are shown in Figs. 2 and 3. PVPh has a glass transition temperature T_g at 157°C. Fig. 3 shows that only blends containing less than 60% PCL (w/w) can yield a single T_g. Glass transition temperature varies with the overall blend composition as indicated by the filled circles in Fig. 4. The existence of a single and compositional dependent T_g implies that the blend exhibits a homogeneous single amorphous phase; i.e. the two polymers are miscible in the amorphous phase. The T_g–composition relationship can be evaluated by the Gordon–Taylor equation [22]

$$T_g = ((W_1 T_{g1} + kW_2 T_{g2})/(W_1 + kW_2)) \quad (1)$$

where T_g is the glass transition temperature of the blends, T_{g1} and T_{g2} are those of pure components, PCL and PVPh, respectively, and k is an adjustable fitting parameter that semi-qualitatively describes the strength of inter-molecular

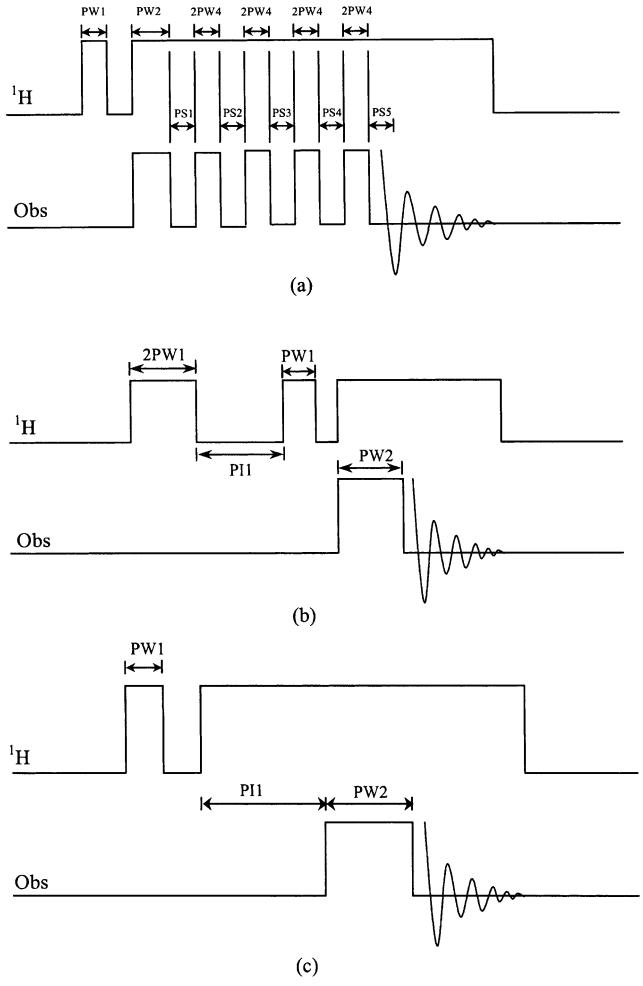

Fig. 1. Pulse sequences used in NMR measurements: (a) sequence for ^{13}C CP/MAS/DD spectra measurement with TOSS; (b) sequence for T_1(H) measurement; (c) sequence for $T_{1\rho}$(H) measurement. Key: PW1, 90° pulse of ^{1}H; PW2, contact time; PW4, 90° pulse of ^{13}C; PI2, delay time; PS1-5, time interval.

interactions. When $k = 1$, T_g would be a simple linear weighted-average of T_{g1} and T_{g2}, indicative of good miscibility between the two components. W is the weight fraction. The dash curve in Fig. 4 was drawn using the Gordon–Taylor equation with a k value of 0.24, which indicates that the inter-molecular interaction between PCL and PVPh is relatively weak compared to other polymer blends [23–26].

Fig. 2 clearly shows the melting endotherms for the blends containing more than 60% PCL (w/w), and crystallization exotherms for the blends containing 60–80% PCL. The PCL90 sample exhibits an extra melting peak at a relatively lower temperature (49°C), compared to that of pure PCL (53°C), and PCL80 shows a shoulder peak at around 47°C. The melting peaks of the PCL70 and PCL60 shift to even lower temperature to about 45°C. The compositional dependence of T_c and T_m of the blends are shown in Fig. 4. The above results indicate that the specific interactions between the two polymers result in the polymer

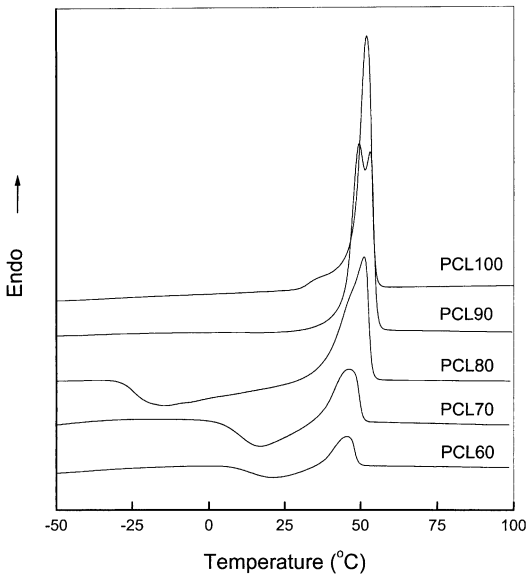

Fig. 2. Second heating scan of DSC thermograms of PCL/PVPh blends containing ≥60% PCL.

chains diffusing into each other's phase, which causes the change of crystallization behaviours of PCL. Hence, the melting transition changed as well. The crystallinity index, X_c, was calculated from the following equation

$$X_c = (\Delta H_f + \Delta H_c)/\Delta H_f^0 \quad (2)$$

where $\Delta H_f^0 = 136$ J/g is the heat of fusion of 100% crystalline PCL [27]. The obtained results for the second heating scan are listed in Table 1. Because the NMR samples did not undergo the heating and quenching process, DSC results from the first heating scan are also presented in Table 2 and Fig. 5 for comparisons. Melting endotherms are

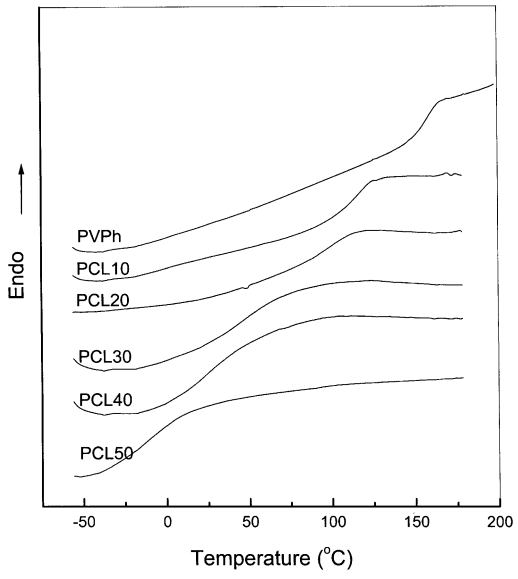

Fig. 3. Second heating scan of DSC thermograms of PCL/PVPh blends containing ≤50% PCL.

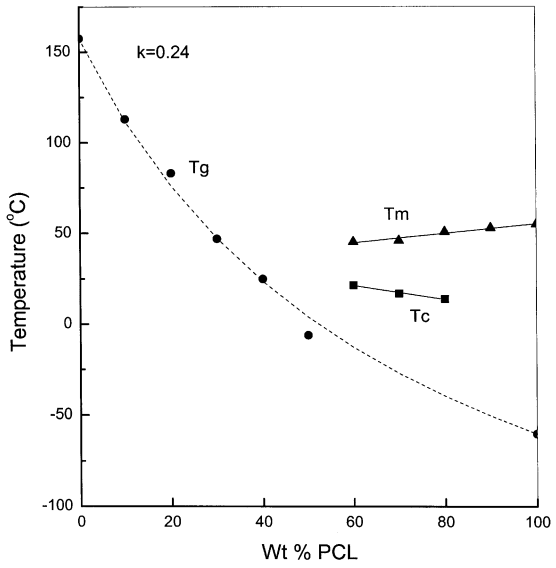

Fig. 4. Thermal transition behavior of the PCL/PVPh blends: (●) T_g versus overall blend composition; (–) calculated T_g curve according to the Gordon–Taylor equation with $k = 0.24$; (▲) T_m; (■) T_c.

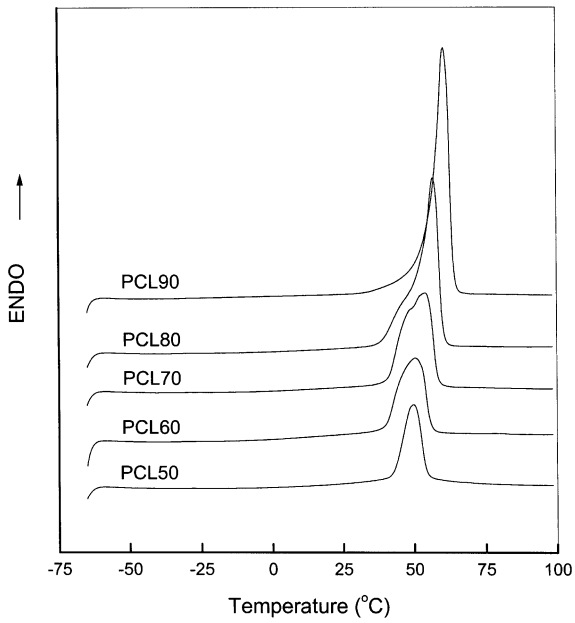

Fig. 5. First heating scan of DSC thermograms of PCL/PVPh blends containing ≥50% PCL.

observed for samples containing more than 50% PCL, but no crystallization exotherms are observed for all samples during the first heating scan. The crystallinity in the unquenched blend samples was calculated using Eq. (2), and is listed in Table 2. It can be seen in Table 2 that samples containing more than 50% PCL have a crystalline phase. In contrast, based on the crystallinity data of quenched samples listed in Table 1, obvious crystalline phase can only be observed for the samples containing more than 80% PCL.

3.2. Fourier transform infrared spectroscopy (FTIR)

Fig. 6 shows FTIR spectra of PCL/PVPh blends in the stretching region of the PVPh hydroxyl groups ranging from 4000 to 2600 cm^{-1}. As shown in curve A, pure PVPh is composed of two vibration bands related to 'free' and intra-associated O–H groups, which appear at 3510 and 3353 cm^{-1}, respectively. Free O–H groups refer to those hydrogen atoms that are not involved in hydrogen bonding, and therefore, they vibrate at a higher frequency than the intra-associated O–H groups. The FTIR absorption peak position shifts from 3355 to 3437 cm^{-1} with increasing PCL content, which indicates that there is inter-molecular hydrogen bonding in the blends.

Fig. 7 shows the FTIR spectra of the carbonyl (C=O) absorbance peak for the PCL/PVPh blends in the region from 1800 to 1640 cm^{-1}. It can be seen from curve A in Fig. 7 that the crystalline C=O absorption peak of pure PCL at 1725 cm^{-1} remains at the same wavenumber for all blend compositions. A shoulder peak can also be observed at 1736 cm^{-1} for pure PCL, which is attributed to the carbonyl groups of the amorphous portion of PCL. Upon blending with PVPh, a new absorption band appeared at 1705 cm^{-1}, corresponding to the hydrogen-bonded carbonyl groups because its intensity increases with increasing PVPh content.

3.3. ^{13}C CP/MAS/DD solid state NMR spectra

The ^{13}C CP/MAS/DD spectra of PCL/PVPh blends are

Table 1
Thermal properties of PCL/PVPh blends for the second heating

PCL/PVPh	T_m (°C)	ΔH_f (J/g_{blend})	ΔH_f (J/g_{PCL})	T_c (°C)	ΔH_c (J/g_{blend})	ΔH_c (J/g_{PCL})	X_c (blend)(%)	X_c (PCL)(%)	T_g (°C)
100/0	55	63.6	63.6				46.8	46.8	− 60
90/10	53	72.2	80.2				59.0	65.6	
80/20	51	51.5	64.4	14	− 43.7	− 54.6	5.7	7.2	
70/30	46	22.2	31.7	17	− 21.7	− 31	0.4	0.5	
60/40	45	10.2	17.0	22	− 9.7	− 16.2	0.4	0.6	
50/50									− 6
40/60									25
30/70									47
20/80									83
10/90									113
0/100									157

Table 2
Thermal properties of PCL/PVPh blends for the first heating

PCL/PVPh	T_m (°C)	ΔH_f (J/g_{blend})	ΔH_f (J/g_{PCL})	X_c (blend)(%)	X_c (PCL)(%)
100/0	59.4	73.4	73.4	0.54	0.54
90/10	60.7	98.4	109.3	0.72	0.80
80/20	56.7	81.6	102	0.60	0.75
70/30	54.1	60.3	86.1	0.44	0.63
60/40	50.4	44.3	73.8	0.33	0.54
50/50	49.8	30.7	61.4	0.23	0.45

shown in Fig. 8. Relative broad resonance for PVPh and sharp resonance for PCL reflect the difference in amorphous and semi-crystalline polymers. Assignments of ^{13}C spectra of PCL and PVPh are shown in Table 3, according to earlier reports in the literature [7,28].

Table 4 shows that the chemical shift of the phenolic C–OH resonance of PVPh varies from 153.8 ppm for the pure PVPh to 154.7 ppm for the PCL70 blend. The C=O resonance of PCL varies from 173.9 ppm for the PCL30 blend to 175.0 ppm for the pure PCL. Together with the observed FTIR absorption peak position changes, the 1 ppm downfield shifting of C–OH resonance and C=O resonance with increasing PCL content suggests that inter-molecular hydrogen bonding occurs between the phenolic hydroxyl proton of PVPh and the carbonyl oxygen of PCL. However, it is important to note that the relatively narrow peak of the PCL C=O resonance at 175 ppm splits into a doublet with increasing PVPh content. The split is due to the difference in relaxation times of the hydrogen-bonded and non-hydrogen-bonded resonances. This doublet should also be realized while examining the relaxation times in Table 6, as discussed next.

3.4. Proton spin–lattice relaxation time

According to the π–τ–$\pi/2$ inversion–recovery scheme, a single T_1(H) relaxation obeys the following equation

$$\ln[(M_e - M_\tau)/(2M_e)] = -\tau/T_1(\mathrm{H}) \quad (3)$$

where T_1(H) is the proton spin–lattice relaxation time in the laboratory frame, τ the delay time used in the experiment, M_τ the corresponding resonance intensity, M_e the intensity at $\tau \geq 5T_1(H)$. Fig. 9 shows the plots of $\ln[(M_e - M_\tau)/(2M_e)]$ versus τ, for the OCH_2 site of PCL at 66 ppm. T_1(H) relaxations at other sites also follow the single exponential relaxation of Eq. (3). Table 5 lists the T_1(H) values at different sites and of different compositions. T_1(H) values of the blends are intermediate to those of the pure polymers. These results indicate that spin diffusion among the protons within the T_1(H) time scale is sufficient to average out the intrinsic spin–lattice relaxation of the different domains. Thus, the domain size of these blends is smaller than the diffusive path length within the T_1(H) time scale. The following one-dimensional diffusion equation may be used to approximate the upper limit of the mixing scale [29–31]:

$$\langle L^2 \rangle = 6DT_i(\mathrm{H}) \quad (4)$$

where D is the spin-diffusion coefficient, which depends on the average proton to proton distance as well as on the dipolar interaction. It has a typical value for polymeric

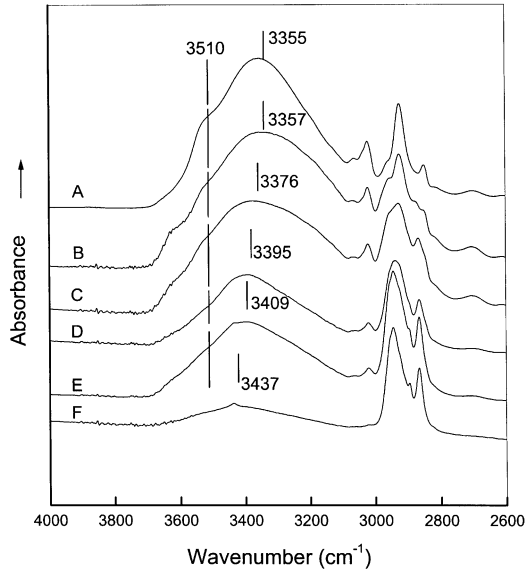

Fig. 6. FTIR spectra in the hydroxyl region of the PCL/PVPh blends: (A) 100, (B) 90, (C) 70, (D) 50, (E) 30 (F) 10 wt% PVPh.

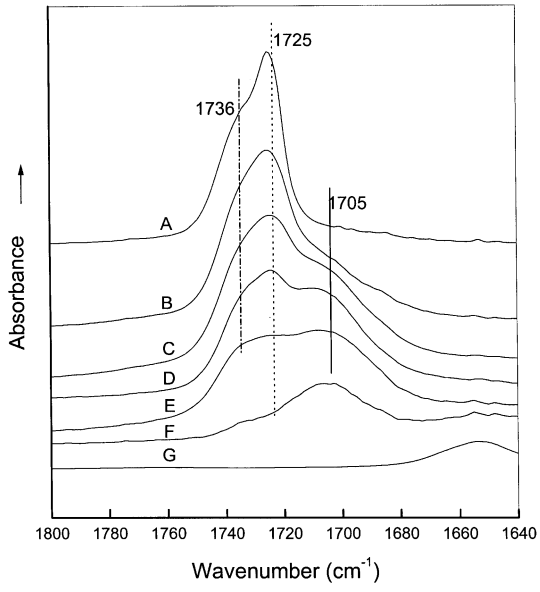

Fig. 7. FTIR spectra in the carbonyl region of the PCL/PVPh blends: (A) 100, (B) 90, (C) 70, (D) 50, (E) 30, (F) 10 (G) 0 wt% PCL.

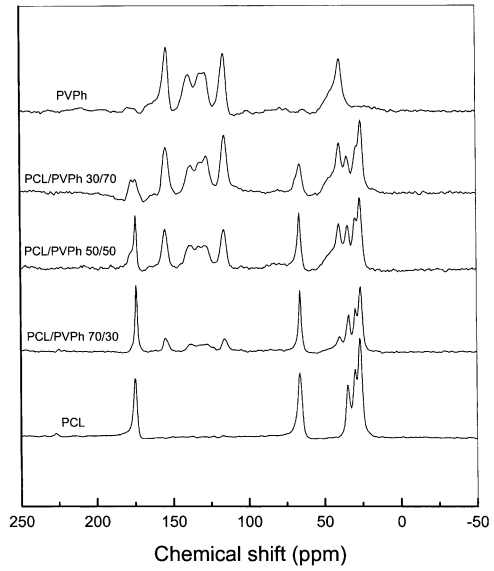

Fig. 8. ^{13}C CP/MAS/DD spectra of the PCL/PVPh blends.

systems in the order of $4–6 \times 10^{-16}$ m^2 s^{-1}. T_i is the relaxation time, T_1(H) or $T_{1\rho}$(H), according to the type of relaxation measurement. On the basis of T_1(H), it is estimated that the two polymers are intimately mixed on a scale of less than 50–80 nm.

3.5. Proton spin–lattice relaxation time in the rotating frame

The spin–lattice relaxation time in the rotating frame $T_{1\rho}$(H) is measured to examine the heterogeneity of the PCL/PVPh blends on the scale of 2–4 nm. A non-single exponential $T_{1\rho}$(H) decay at the OCH_2 site of PCL is observed in Fig. 10 because PCL is a semi-crystalline polymer. A bi-exponential decay function is used to fit the data

$$M_\tau = M_{0,\text{fast}} \exp\left(\frac{-\tau}{T_{1\rho,\text{fast}}(\text{H})}\right) + M_{0,\text{slow}} \exp\left(\frac{-\tau}{T_{1\rho,\text{slow}}(\text{H})}\right) \quad (5)$$

Table 4
^{13}C chemical shifts (ppm) of PCL/PVPh blends

PCL/PVPh	PCL C=O	PVPh COH
0/100		153.8
30/70	173.9	153.9
50/50	174.0	154.3
70/30	173.9	154.7
100/0	175.0	

The $T_{1\rho}$(H) values of the PCL/PVPh blends were calculated from Eq. (5), and the results are listed in Table 6. $T_{1\rho}$(H) relaxation of PVPh is a single exponential because PVPh is an amorphous polymer. The fraction of the intensity of the slow decay component $M_{0,\text{slow}}$ over the total intensity M_0 is calculated, and the results are listed in Table 7. The fraction ($M_{0,\text{slow}}/M_0$) increases with increasing PCL content, and shows the same trend as the crystallinity in the un-quenched samples of Table 2. The PCL $T_{1\rho}$(H) values of the fast decay component are almost the same as the PVPh $T_{1\rho}$(H) values, which suggests that the amorphous phase of PCL is miscible with PVPh. Therefore, it can be concluded that the slow decay component corresponds to the rigid crystalline phase of PCL, while the fast one corresponds to the amorphous phase of PCL. Since the amorphous PCL decays have relaxation times similar to that of PVPh, the hydrogen bonds are expected from the structure analysis. The occurrence of the doublet of C=O resonance in Fig. 8 is most probably due to the hydrogen bonding effect.

Both DSC (Table 2) and NMR data (Table 7) show that if the PVPh content in the blend is less than 30%, the PCL crystallinity is even higher than that of pure PCL. This is probably because the phenolic groups of PVPh serve as nucleation sites for the crystallization of PCL. The crystallinity listed in Table 2 is slightly different from that listed in Table 7 because the value determined with DSC is based on the quantity of heat energy needed to melt the crystals; whereas, the crystallinity determined with NMR is based

Table 3
Assignment of ^{13}C CP/MAS spectra of PCL, PVPh at 300 K

Compound	Structure	Carbon	Assignment
PCL	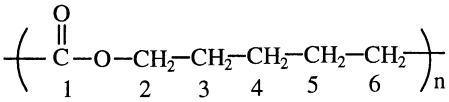	1	175.0
		2	66.0
		3	29.8
		4,5	26.7
		6	34.8
PVPh	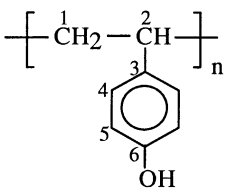	1,2	40.3
		3	138.5
		4	128.2
		5	116.2
		6	153.8

Table 5
$T_1(H)$ values (s) for PCL, PVPh and their blends (ND stands for not detected due to low single-to-noise ratio)

Composition (PCL wt%)	PVPh		PCL	
	COH 154 ppm	CH 116 ppm	OCH_2 66 ppm	CH_2 27 ppm
0	1.48	1.32	–	–
30	1.27	1.33	1.38	ND
50	1.24	1.23	1.30	1.21
70	1.14	1.18	1.06	1.11
100	–	–	0.82	0.80

Table 6
$T_{1\rho}(H)$ values (ms) for PCL, PVPh and their blends (ND stands for not detected due to low single-to-noise ratio)

Composition (PCL wt%)	PVPh		PCL	
	COH 154 ppm	CH 116 ppm	OCH_2 66 ppm	CH_2 27 ppm
0	7.6	6.8	–	–
30	9.2	8.3	8.6/98.1	7.9/108.0
50	4.9	5.8	6.0/55.0	4.8/47.5
70	3.7	4.7	6.0/50.7	4.6/47.8
100			14.0/47.6	8.9/43.7

on differences in chain mobility of the rigid crystalline phase and of the mobile amorphous phase. Systematic errors in curve fitting NMR data with Eq. (5) also contribute to the differences in crystallinity determined by both methods. Even though Eq. (5) is used for the PCL30 sample, the fraction ($M_{0,slow}/M_0$) calculated for the OCH_2 (66 ppm) and CH_2 (27 ppm) sites are 0.14 and 0.06, respectively. Fractions that are below 0.15 are not reliable because baseline noises would contribute significant errors to the slow decay component. The slow $T_{1\rho}(H)$ decay component of the PCL30 sample is unlikely to be crystalline because DSC thermograms show that the blends with less than 50% PCL are amorphous.

4. Conclusions

DSC measurements reveal that the PCL/PVPh blends are composed of a crystalline and an amorphous phase. The blends containing less than 50% PCL are amorphous. The glass transition temperature of the blends containing more than 50% PCL cannot be detected, but their melting transitions shift to lower temperatures with increasing PVPh concentration. It is found that PVPh can enhance PCL crystallinity in certain conditions.

FTIR results indicate that hydrogen bonding exists

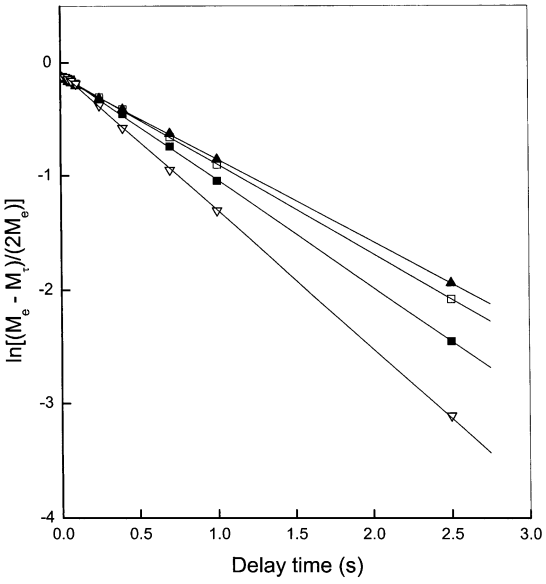

Fig. 9. Logarithmic plot of resonance intensity (at 66 ppm) vs. delay time to measure T_1(H). PCL/PVPh: (▲) 30/70, (□) 50/50, (■) 70/30 (▽) 100/0.

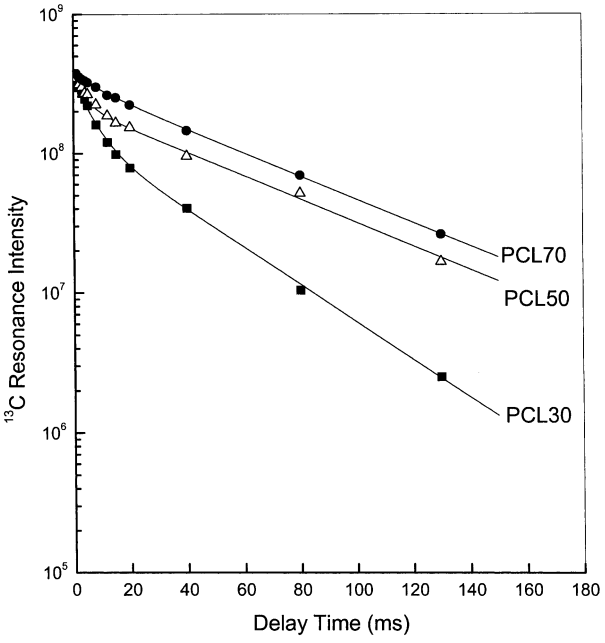

Fig. 10. Logarithmic plot of resonance intensity (at 66 ppm) vs. delay time to measure $T_{1\rho}$(H). PCL/PVPh: (●) 70/30, (△) 50/50, (■) 30/70.

Table 7
Degree of PCL crystallinity measured from the fraction of the long $T_{1\rho}$(H) component $M_{0,\ slow}$ to that of the total decay M_0

$M_{0,\ slow}/M_0$	OCH_2 66 ppm	CH_2 27 ppm
PCL50	0.56	0.44
PCL70	0.76	0.77
PCL100	0.62	0.57

between the phenolic hydroxyl groups and the carbonyl groups of PCL. Significant vibrational frequency shifts of the hydroxyl groups of PVPh, and a new absorption band formed in the carbonyl group region of PCL support the idea of hydrogen bonding formed in the blends.

1 ppm downfield shifting of the PVPh hydroxyl-substituted carbons and the PCL carbonyl carbons with increasing PCL content are observed in the solid state ^{13}C CP/MAS/DD spectra, which reveal specific inter-molecular interaction exists between the two polymers. A bi-exponential decay of PCL component is observed in the $T_{1\rho}$(H) measurements, which indicates the presence of crystalline and amorphous phases. From T_1(H) and $T_{1\rho}$(H) measurements, it can be concluded that PCL/PVPh blends are homogeneous on the scale of 50–80 nm, but are heterogeneous on the scale of 2–4 nm. The doublet of the C=O resonance was observed upon adding PVPh, and the carbonyl doublet maybe caused by hydrogen bonding.

Acknowledgements

Research grants RGC HKUST 6120/99P and CMI 99/00.EG03 are greatly acknowledged.

References

[1] Chen HL, Liaw DJ, Liaw BY, Tsai JS. Polym J 1998;30:874.
[2] Zhou H, Xiang M, Chen W, Jiang M. Macromol Chem Phys 1997;198:809.
[3] Sanchis A, Prolongo MG, Salom C, Masegosa RM. J Polym Sci, Part B: Polym Phys 1998;36:95.
[4] Kwak SY. J Appl Polym Sci 1994;53:1823.
[5] De Kesel C, Lefèvre C, Nagy JB, David C. Polymer 1999;40:1969.
[6] Zhang X, Tagegoshi K, Hikichi K. Macromolecules 1992;25:2336.
[7] Zhong Z, Guo Q, Mi Y. Polymer 1998;40:27.
[8] Guo Q, Zheng S, Li J, Mi Y. J Polym Sci, Part A: Polym Chem 1997;35:211.
[9] Mandal TK, Woo EM. Polym J 1999;31:226.
[10] McMaster LP. Adv Chem Ser 1975;43:142.
[11] McBrierty VJ, Packer KJ. Nuclear magnetic resonance in solid polymer. Cambridge: Cambridge University Press, 1993.
[12] Mathias LJ, editor. Solid state NMR of polymer. New York: Plenum Press, 1991.
[13] Zhang X, Takegoshi K, Hikichi K. Polymer 1992;33:712.
[14] Qin C, Priesm ATN, Belfiore LA. Polym Commun 1990;31:177.
[15] Miyoshi T, Takegoshi K, Hikichi K. Polymer 1997;38:2315.
[16] Coleman MM, Lichkus AM, Painter PC. Macromolecules 1989;22:211.
[17] Goh SH, Siow KS. Polym Bull 1987;17:453.
[18] Hong J, Goh SH, Lee SY, Siow KS. Polymer 1995;36:143.
[19] Iriondo P, Iruin JJ, Fernandez-Berridi MJ. Polymer 1995;36:3235.
[20] Iriondo P, Iruin JJ, Fernandez-Berridi MJ. Macromolecules 1996;29:5605.
[21] Belfiore LA, Qin C, Ueda E, Pires ATN. J Polym Sci, Part B: Polym Phys 1993;31:409.
[22] Gordon M, Isasi JR, Katime I. J Polym Sci, Part B: Polym Phys 1994;32:223.
[23] Cesteros LC, Isasi JR, Katime I. J Polym Sci, Part B: Polym Phys 1994;32:223.
[24] Lin P, Clash C, Pearce EM, Kwei TK. J Polym Part B: Polym Phys 1994;32:223.
[25] Zheng S, Wang J, Guo Q, Wei J, Li J. Polymer 1996;37:4667.
[26] Cheung MK, Wang J, Zheng S, Mi Y. Polymer 2000;41:1469.
[27] Khambatta FB, Warmer F, Stein RS. J Polym Sci, Polym Phys Ed 1976;14:1391.
[28] Jack KS, Whittaker AK. Macromolecules 1997;30:3560.
[29] McBrierty VJ, Douglass DC. J Polym Sci Macromol Rev 1981;16:295.
[30] Demco DE, Johannsson A, Tegenfeldt J. Solid State Nucl Magn Reson 1995;4:13.
[31] Clauss J, Schmidr-Rohr K, Spiess HW. Acta Polym 1993;44:1.